Ternary superconducting hydrides in the La–Mg–H system

Grigoriy M. Shutov [a,*], Dmitrii V. Semenok [b], Ivan A. Kruglov [c,d], Artem R. Oganov [a]

[a] *Skolkovo Institute of Science and Technology, Moscow, 121205, Russia*
[b] *Center for High Pressure Science and Technology Advanced Research (HPSTAR), Beijing, 100094, China*
[c] *Moscow Institute of Physics and Technology, Dolgoprudny, 141700, Moscow Oblast, Russia*
[d] *Dukhov Research Institute of Automatics (VNIIA), Moscow, 127055, Russia*

ARTICLE INFO

ABSTRACT

Ternary or more complex hydrogen-rich hydrides are the main hope of reaching room-temperature superconductivity at high pressures. Their chemical space is vast and its exploration is challenging. Here we report the investigation of the La–Mg–H ternary system using the evolutionary algorithm USPEX at pressures in the range 150–300 GPa. Several ternary superconducting hydrides were found, including thermodynamically stable $P6/mmm$-LaMg$_3$H$_{28}$ with $T_C = 164$ K at 200 GPa, $P/2m$-LaMgH$_8$, $C2/m$-La$_2$MgH$_{12}$ and $P2/m$-La$_3$MgH$_{16}$. In addition, novel binary hydrides were predicted to be stable at various pressures, such as Cm–Mg$_6$H$_{11}$, $P1$–MgH$_{26}$, $Fmm2$-MgH$_{30}$, $P1$–MgH$_{38}$ and $R\overline{3}m$-LaH$_{13}$. We also report several novel low-enthalpy metastable phases, both ternary and binary ones. Finally, we demonstrate important methods of exploring very large chemical spaces and show how they can improve crystal structure prediction.

1. Introduction

The highest-temperature superconductors know today are polyhydrides - hydrides anomalously rich in hydrogen (above what can be expected based on atomic valences). They were anticipated with the hypothesis proposed by Ashcroft [1] that hydrogen-rich materials can become superconductors at high pressures. Some hydride systems demonstrate high superconducting critical temperature, such as $Im\overline{3}m$-H$_3$S with $T_C = 203$ K [2], $Fm\overline{3}m$-LaH$_{10}$ with $T_C = 250$ K [3,4], $P6_3/mmc$-ThH$_9$ and $Fm\overline{3}m$-ThH$_{10}$ with $T_C = 146$ K and $T_C = 159 - 161$ K [5], respectively, and $Im\overline{3}m$-YH$_6$ with $T_C = 224 - 226$ K [6].

Semenok et al. [7] showed that highest-T_C superconducting hydrides are formed by elements of II-III groups, such as calcium, strontium, barium, scandium, yttrium, lanthanum , cerium and thorium. Elements grouped near these (and to a lesser extent near sulfur) in the periodic table often form binary hydrides with the $T_C > 100$ K.

The search continues in ternary systems, as ternary hydrides have several advantages compared to binary hydrides. First, such hydrides may have potentially higher T_C. For example, $T_C = 253$ K has been reported for (La,Y)H$_{10}$ [8], compared to $T_C = 250$ K of LaH$_{10}$ [3,4]. Second, ternary hydrides can have lower stabilisation pressure, as it is shown for La–Ce–H [9,10], La–Be–H [11] and La–B–H systems [12,13]. Overall, ternary systems provide much more space for the search.

Among all binary systems, only a few have high-T_C superconducting hydrides and correspond to the "lability belt" [7], whereas in the space of ternary systems there are dozens of possible combinations of the best binary ones.

As $T_C = 250$ K of LaH$_{10}$ has been proven experimentally [3,4], we can presume that ternary hydrides of lanthanum and some other element may also be high-temperature superconductors. In this work, we study phases formed by lanthanum, magnesium and hydrogen and their superconducting properties.

Lanthanum hydrides have been theoretically predicted to form several phases at high pressures: $P6/mmm$-LaH$_2$, $Cmmm$-La$_3$H$_{10}$, $I4/mmm$-LaH$_4$, $C2/m$- and $Fm\overline{3}m$-LaH$_{10}$, and $P6/mmm$-LaH$_{16}$ [14]. Moreover, experimental synthesis revealed seven phases of binary lanthanum hydrides [15]. According to predictions, LaH$_{10}$ is a superconductor with $T_C = 274 - 286$ K [16]. Magnesium hydrides also form four phases at 200 GPa: $P6_3/mmc$-MgH$_2$, $Cmcm$-MgH$_4$, $R\overline{3}$-MgH$_{12}$, and $P1$-MgH$_{16}$. However, they have relatively low reported T_C: 29–37 K for MgH$_4$ and 20 K for MgH$_2$ and 47–60 K for MgH$_{12}$. For MgH$_{16}$, T_C has not been calculated [17]. Another study reports $Im\overline{3}m$-MgH$_6$ with $T_C = 260$ K at pressure above 300 GPa [18].

In this work, we use the evolutionary algorithm USPEX [19–21] to study the chemical space of the La–Mg–H system. For more detailed search of La–Mg–H ternary hydrides, we additionally perform

---

evolutionary searches on the pseudobinary sections formed by Mg–H and La–H binary hydrides.

2. Methods

The evolutionary algorithm USPEX [19–21] was used to predict thermodynamically stable phases. To investigate the La–Mg–H system, we performed both fixed- and variable-composition searches at 200 GPa.

One of the possible straightforward ways to search for new stable hydrides in La–Mg–H system is to perform USPEX calculations in the ternary system. However, such search requires large computational resources, because the chemical space of ternary systems is huge. To tackle this problem, we performed variable-composition searches on special pseudobinary sections of the convex hull with LaH_x–MgH_y ($x = 2, 4, 10, 16$, $y = 2, 4, 12, 16$) composition blocks. In addition, we performed variable-composition searches with such composition blocks as LaH_x–Mg and La–MgH_y ($x = 2, 4, 10, 16$, $y = 2, 4, 12, 16$ as well). The parameters of each search are presented in Supplementary Materials, Table S1.

After studying the pseudobinary sections, the ternary variable-composition search at 200 GPa pressure was performed, using previously found structures as seeds. The number of generations in this evolutionary search was 100. After this search, several ternary hydrides remained on the convex hull. Moreover, novel binary hydrides were discovered. Using stable and metastable structures at the pressure of 200 GPa as seeds, ternary convex hulls were also calculated at 150, 250 and 300 GPa. Additionally, we recalculated these ternary convex hulls on the temperature range from 0 K to 2000 K, using free energies computed by Phonopy. Metastable structures with the energy above convex hull $E_{Hull} \leq 10$ meV/atom are also presented on each convex hull plot in this work.

Structure relaxations and energy estimation were performed using the VASP code [22–24] within density functional theory (DFT) [25,26], using the Perdew–Burke–Ernzerhof (PBE) exchange–correlation functional [27] and the projector-augmented wave (PAW) method [28,29]. The kinetic energy cutoff was set at 600 eV. Γ-centered k-point meshes with a resolution of $2\pi \times 0.05$ Å^{-1} were used for sampling the Brillouin zone.

The phonon band structure and density of states were computed using Phonopy [30] package implementing the finite displacement method. $2 \times 2 \times 2$ supercells were generated. The energy cutoff and k-spacing parameters for VASP calculations were set at 500 eV and $2\pi \times 0.1$ Å^{-1}, respectively. Sumo package [31] was used to visualize the phonon density of states and band structure. The k-points for phonon band structures were chosen using Hinuma's recommendation [32]. The Phonopy package was also used to calculate zero-point energy (ZPE) corrections and thermal properties, such as the entropy and free energy. In addition, space group symmetries were also investigated by the Phonopy package. Some of the predicted structures can be symmetrized to various space groups depending on the tolerance parameter. We chose the maximum symmetry space groups within whose structures exhibited dynamical stability.

To calculate phonon frequencies and electron–phonon coupling (EPC) coefficients, we used Quantum Espresso (QE) package [33] utilizing density functional perturbation theory (DFPT) [34], plane-wave pseudopotential method, and the PZ-HGH [35,36] pseudopotentials. The q-meshes for each structure were $3 \times 3 \times 3$, except MgH_{26}, MgH_{30} and MgH_{38}, for which it was set to $2 \times 2 \times 2$. The Allen–Dynes [37] formula was used to calculate T_C:

$$T_C = \omega_{\log} \frac{f_1 f_2}{1.2} \exp\left[\frac{-1.04(1 + \lambda)}{\lambda - \mu^* - 0.62\lambda\mu^*}\right]. \tag{1}$$

The McMillan formula has the term $f_1 f_2 = 1$, whereas in the Allen–Dynes formula, it is expressed as:

$$f_1 f_2 = \sqrt[3]{1 + \left[\frac{\lambda}{2.46(1 + 3.8\mu^*)}\right]^{3/2}} \cdot \left[1 - \frac{\lambda^2(1 - \omega_2/\omega_{\log})}{\lambda^2 + 3.312(1 + 6.3\mu^*)^2}\right], \tag{2}$$

where μ^* is the Coulomb pseudopotential, with the values in the commonly accepted range from 0.10 to 0.15; λ, ω_2, and $\omega_{\log}$ are the EPC constant, mean square frequency, and logarithmic average frequency, respectively, defined as:

$$\lambda = \int_0^{\omega_{\max}} \frac{2\alpha^2 F(\omega)}{\omega} d\omega, \tag{3}$$

$$\omega_{\log} = \exp\left[\frac{2}{\lambda} \int_0^{\omega_{\max}} \frac{d\omega}{\omega} \alpha^2 F(\omega)\log(\omega)\right], \tag{4}$$

$$\omega_2 = \sqrt{\frac{1}{\lambda} \int_0^{\omega_{\max}} \left[\frac{2\alpha^2 F(\omega)}{\omega}\right] \omega^2 d\omega}. \tag{5}$$

where $\alpha^2 F(\omega)$ is an Eliashberg function.

Moreover, full solution of Eliashberg equations [38] was computed using Allen's algorithm [39]. This algorithm was implemented in our code published on GitHub [40].

To estimate the thermodynamic properties such as thermodynamic critical magnetic field H_C, superconducting gap $\Delta(0)$ and specific heat jump $\Delta C(T_c)$, we used the semiempirical formulas [41]:

$$\frac{\gamma T_C^2}{H_C^2(0)} = 0.168\left[1 - 12.2\left(\frac{T_C}{\omega_{\log}}\right)^2 \ln\left(\frac{\omega_{\log}}{3T_C}\right)\right], \tag{6}$$

$$\frac{2\Delta(0)}{k_B T_C} = 3.53\left[1 + 12.5\left(\frac{T_C}{\omega_{\log}}\right)^2 \ln\left(\frac{\omega_{\log}}{2T_C}\right)\right], \tag{7}$$

$$\frac{\Delta C(T_c)}{\gamma T_c} = 1.43\left[1 + 53\left[\frac{T_c}{\omega_{\log}}\right]^2 \ln\left[\frac{\omega_{\log}}{3T_c}\right]\right], \tag{8}$$

where k_B is the Boltzmann constant and $\gamma = \frac{2}{3}\pi^2 k_B^2 N(0)(1 + \lambda)$ is the Sommerfeld. The values of T_C from the solution of Eliashberg equations were used in these formulas.

We note that lower and upper critical magnetic fields H_{C1} and H_{C2} are related to H_C by the following equation:

$$H_C = \frac{\sqrt{H_{C1}H_{C2}}}{\sqrt{\ln \kappa}} \tag{9}$$

where κ is Ginzburg-Landau parameter, and that H_{C2} is usually one or two orders of magnitude higher than H_C. For example, $\kappa = 20$, $H_{C1} = 0.55$ T and $H_{C2} = 143.5$ T were reported for $Fm\bar{3}m$-LaH_{10} [42], leading to $H_C = 5.13$ T. Formula (6) returns $H_C = 6.7$ T, which is close to the experimental value.

3. Results

As a result of the variable-composition searches with LaH_x–MgH_y ($x = 2, 4, 10, 16$, $y = 2, 4, 12, 16$) composition blocks at 200 GPa, 13 ternary phases were found to be stable with respect to their pseudobinary section (see Table S1). After variable-compostion searches in LaH_x–Mg and La–MgH_y ($x = 2, 4, 10, 16$, $y = 2, 4, 12, 16$ as well) pseudobinary sections, 20 ternary phases were discovered, and some of them were metastable on the ternary convex hull. Other thermodynamically stable phases for each pseudobinary section are presented in Table S1.

Ternary convex hulls and phase diagrams, recalculated with ZPE correction on $P = 150, 200, 250$ and 300 GPa, are presented in Fig. 1. They revealed $P/2m$-$LaMgH_8$, $C2/m$-La_2MgH_{12} and $P6/mmm$-$LaMg_3H_{28}$ that are stable at $P = 200, 250$ and 300 GPa and $P2/m$-La_3MgH_{16} that is
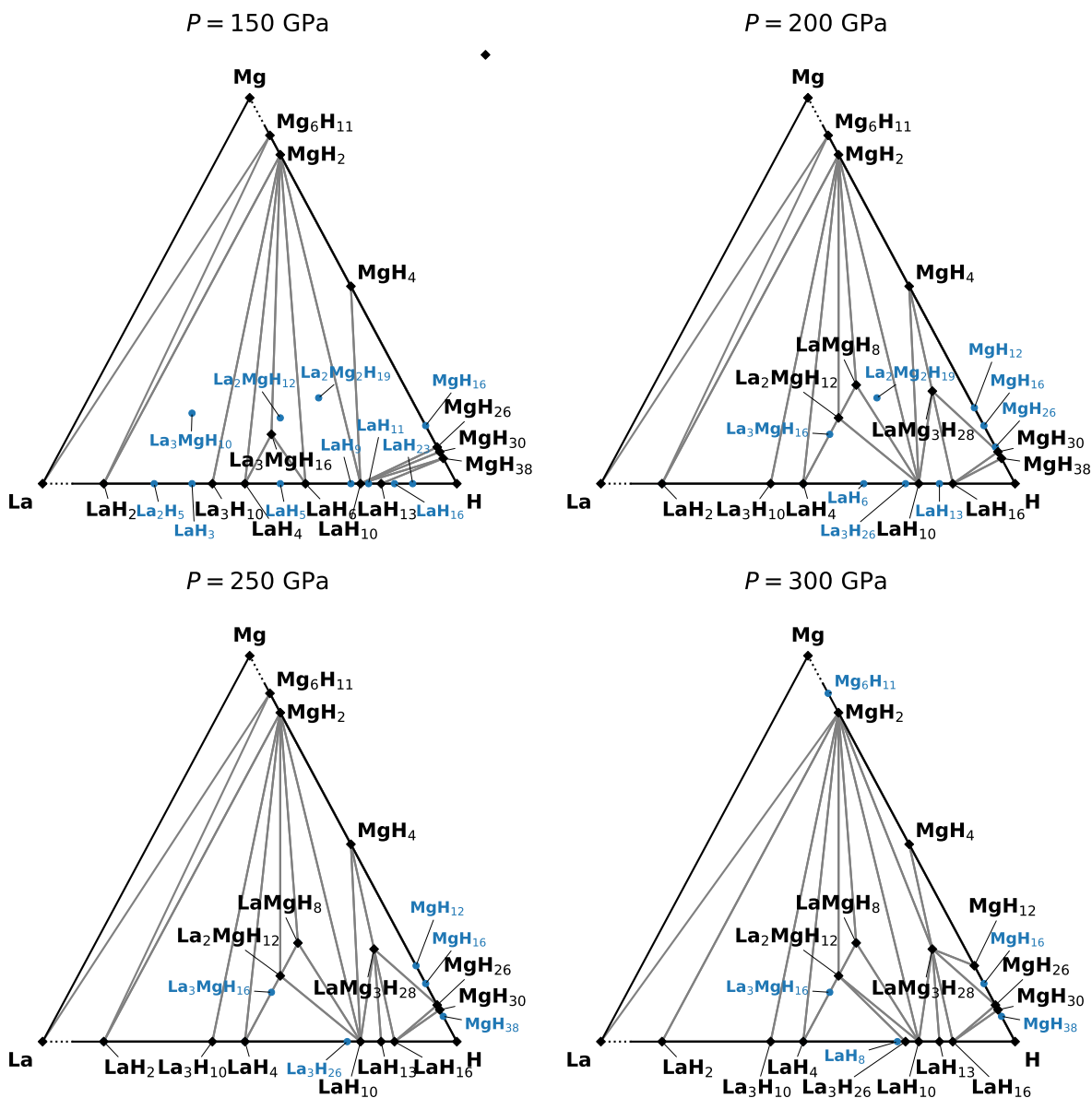
Fig. 1. Convex hulls and phase diagrams of the La–Mg–H system, recalculated with zero-point energy (ZPE) corrections. The black diamonds are stable structures, the blue circles are metastable ones with the $E_{\text{Hull}} \leq 10$ meV/atom. (For interpretation of the references to colour in this figure legend, the reader is referred to the Web version of this article.)

stable at $P = 150$ GPa.

Additionally, ternary variable-composition search at 200 GPa revealed novel binary lanthanum and magnesium hydrides: $R\overline{3}m$-LaH$_{13}$, $C2/m$-LaH$_{23}$, Cm–Mg$_6$H$_{11}$, $P1$–MgH$_{26}$, $Fmm2$-MgH$_{30}$ and $P1$–MgH$_{38}$.

Convex hulls and phase diagrams at non-zero temperatures are presented in Supplementary materials (see Figs. S1–S4). Crystal structures are presented in Table S2.

We note that since lanthanum and magnesium atoms have very different properties, they do not form solid solutions in the La–Mg system. This is confirmed by the structures of predicted ternary hydrides: difference in lanthanum and magnesium elements' properties results in very different coordination numbers and hydrogen cage shapes (see Section 3.2).

3.1. Novel binary hydrides

Novel binary lanthanum hydride $R\overline{3}m$-LaH$_{13}$ (see Fig. 2a) is thermodynamically stable at the pressures 200 GPa and 250 GPa. At 250

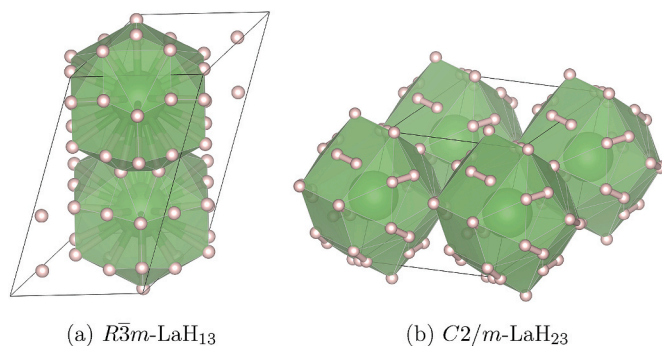(a) $R\overline{3}m$-LaH$_{13}$ (b) $C2/m$-LaH$_{23}$

Fig. 2. Crystal structures of novel lanthanum binary hydrides (visualized by VESTA software [44]).

GPa, its H–H distances are 0.90 Å while its average La–H distace is 2.02 Å. It is interesting to note that this phase can shed light on the solution of the long-standing problem of the LaH$_{12}$ structure, found experimentally, but not yet theoretically explained [3,43].

As demonstrated in Table 1, predicted T_C of LaH$_{13}$ is higher than 100 K. However, it is lower than T_C of LaH$_{10}$ (T_C = 250 K [3,4]). The low symmetry of LaH$_{13}$ and the molecular sublattice of hydrogen result in low electron-phonon coupling parameters. Molecular hydrogen makes a low contribution to DOS due to the strong localization of s-electrons in the σ-orbital of H$_2$ molecules. At the same time, the main contribution to the phonon DOS lies in the collective vibrations of the H$_2$ and H$_3$ molecules around their equilibrium positions, which practically does not affect the length of the H–H bonds and does not change the localization of s-electrons in σ-orbitals. In addition, electron transfer per atom for LaH$_{13}$ is 0.231e, while high-temperature superconductors like LaH$_{10}$ and YH$_9$ usually have transfer about 0.33e [45].

Another novel lanthanum hydride $C2/m$-LaH$_{23}$ (see Fig. 2b) is metastable by 6.8 meV/atom at P = 150 GPa. It contains H$_2$ molecules with H–H distances from 0.77 Å to 0.89 Å. Its average La–H distance is 2.12 Å. At P = 150 GPa it has T_C = 85.1 K. At P = 200 GPa its T_C increases up to 100.5 K, however, its E_{Hull} also increases to 12 meV/atom. The reason of superconductivity in LaH$_{23}$ is the partial metallization of the

hydrogen sublattice. According to recent experimental results, metallization of hydrogen happens at extremely high pressures above 400 GPa [46]. However, such in accordance with Ashcroft 's hypothesis [1] metallization is observed in binary hydrides at much lower pressures and T_C of such hydrides increases with the increase of pressure. This was previously confirmed in the experimental study of metallization and superconductivity of BaH$_{12}$ [47].

Like previously reported [17] $R\bar{3}$-MgH$_{12}$ and $P\bar{1}$-MgH$_{16}$, novel magnesium hydrides $P1$-MgH$_{26}$, $Fmm2$-MgH$_{30}$ and $P1$-MgH$_{38}$ contain molecular hydrogen. As demonstrated in Fig. 3(a–c), their unit cells contain discrete H$_2$ molecules. Moreover, Mg atoms are surrounded by belts of 6H$_2$ molecules, similarly to MgH$_{12}$ and MgH$_{16}$. Average H–H distances are 0.77 Å, 0.77 Å and 0.76 Å for MgH$_{26}$, MgH$_{30}$ and MgH$_{38}$, respectively. Mean Mg–H distances are 1.74 Å, 1.74 Å and 1.75 Å for MgH$_{26}$, MgH$_{30}$ and MgH$_{38}$, respectively. All novel magnesium hydrides have similar structures (see Fig. 3) and similar parameters of their superconducting state, including low T_Cs (see Table 1). These molecular magnesium hydrides are similar to the previously discovered polyhydrides of strontium SrH$_{22}$ [48], barium BaH$_{12}$ [47], cesium CsH$_{15-17}$ [49], and rubidium RbH$_9$ [50].

3.2. Ternary La–Mg–H hydrides

Using ternary convex hulls, recalculated with zero-point energy correction, we found two novel ternary hydrides (Fig. 1): $C2/m$-La$_2$MgH$_{12}$ at pressures 150 GPa, 200 GPa and 250 GPa and $P6/mmm$-LaMg$_3$H$_{28}$ at 200 GPa and 250 GPa. In La$_2$MgH$_{12}$, La and Mg have coordination numbers 20 and 15, respectively. LaMg$_3$H$_{28}$ has La and Mg coordination numbers 30 and 20, respectively (see Fig. 5). In comparison to $C2/m$-La$_2$MgH$_{12}$, it is hydrogen-rich and has high symmetry.

LaMgH$_8$, La$_2$MgH$_{12}$ and La$_3$MgH$_{16}$ lie at the same pseudobinary section of the convex hull: LaH$_4$–MgH$_4$ (see Fig. 1). LaMgH$_8$, La$_2$MgH$_{12}$ are thermodynamically stable at pressures 200 GPa, 250 GPa and 300 GPa. At pressure of 150 GPa, they become metastable while La$_3$MgH$_{16}$ becomes stable. As shown in on Fig. 5, they share same La–H and Mg–H

Table 1
Superconducting parameters of novel binary hydrides.

Parameter	LaH$_{13}$ 200 GPa	LaH$_{13}$ 250 GPa	LaH$_{13}$ 300 GPa	LaH$_{23}$ 150 GPa	LaH$_{23}$ 200 GPa
λ	1.42	1.69	1.60	0.97	1.11
ω_{log}, K	906	812	1105	1195	1059
ω_2, K	1454	1505	1669	1819	1844
T_C (McM), K	98	103	134	79	86
T_C (A-D), K	118	137	164	87	99
T_C (E), K	131	155	172	85	101
N_f, $\frac{states}{Ry \cdot Å^3}$	0.091	0.097	0.101	0.091	0.096
γ, $\frac{mJ}{cm^3 \cdot K^2}$	0.126	0.150	0.152	0.103	0.116
$\frac{\Delta C}{T_C}$, $\frac{mJ}{cm^3 \cdot K^2}$	0.347	0.445	0.430	0.208	0.265
$\Delta(0)$, meV	26.4	34.0	35.6	14.5	18.2
$\frac{2\Delta(0)}{k_B T_C}$	4.67	5.08	4.78	3.97	4.19
$H_C(0)$, Tesla	1.7	2.2	2.6	1.0	1.1
Electron transfer, e per H atom	0.231	0.231	0.231	0.130	0.130

Parameter	Mg$_6$H$_{11}$ 200 GPa	MgH$_{26}$ 200 GPa	MgH$_{30}$ 200 GPa	MgH$_{38}$ 200 GPa
λ	0.53	0.55	0.59	0.51
ω_{log}, K	898	1282	979	1002
ω_2, K	1332	2273	2179	2167
T_C (McM), K	14	22	22	13
T_C (A-D), K	14	23	23	14
T_C (E), K	14	23	20	12
N_f, $\frac{states}{Ry \cdot Å^3}$	0.058	0.071	0.064	0.054
γ, $\frac{mJ}{cm^3 \cdot K^2}$	0.051	0.063	0.059	0.047
$\frac{\Delta C}{T_C}$, $\frac{mJ}{cm^3 \cdot K^2}$	0.076	0.095	0.090	0.069
$\Delta(0)$, meV	2.2	3.5	3.2	1.8
$\frac{2\Delta(0)}{k_B T_C}$	3.57	3.58	3.59	3.55
$H_C(0)$, Tesla	0.1	0.2	0.2	0.1
Electron transfer, e per H atom	1.091[a]	0.077	0.067	0.053

T_C was calculated using McMillan (McM), Allen-Dynes (A-D) formulas, and numerical solution of Eliashberg equations (E) with the Coulomb pseudopotential μ^* = 0.1.

[a] one hydrogen atom can accept not more than one electron. Numbers greater than 1 indicate the presence of bonds between metal atoms.

(a) $P1$-MgH$_{26}$ (b) $P1$-MgH$_{38}$

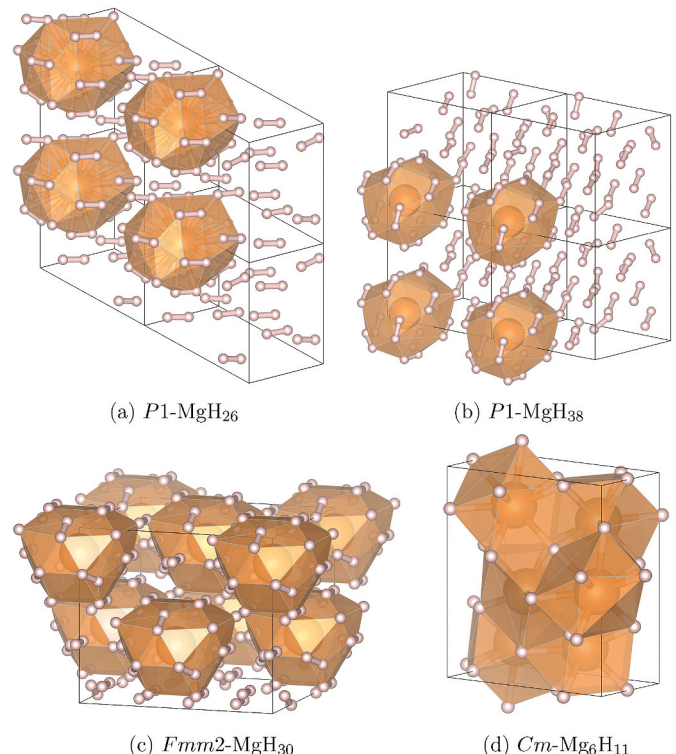(c) $Fmm2$-MgH$_{30}$ (d) Cm-Mg$_6$H$_{11}$

Fig. 3. Crystal structures of novel magnesium binary hydrides.

Table 2
Superconducting parameters of ternary La–Mg–H hydrides.

Parameter	LaMgH$_8$ 200 GPa	LaMgH$_8$ 250 GPa	LaMgH$_8$ 300 GPa	La$_2$MgH$_{12}$ 200 GPa	La$_2$MgH$_{12}$ 250 GPa	La$_2$MgH$_{12}$ 300 GPa
λ	0.74	0.70	0.67	0.60	0.62	0.68
$\omega_{\log}$, K	1014	1195	1277	1042	1172	1014
ω_2, K	1642	1778	1866	1744	1927	1889
T_C (McM), K	41	42	40	24	29	33
T_C (A-D), K	44	44	42	25	31	35
T_C (E), K	43	45	38	24	30	32
N_f, $\frac{\text{states}}{\text{Ry·Å}^3}$	0.115	0.104	0.096	0.111	0.114	0.142
γ, $\frac{\text{mJ}}{\text{cm}^3\cdot\text{K}^2}$	0.116	0.102	0.092	0.102	0.106	0.137
$\frac{\Delta C}{T_C}$, $\frac{\text{mJ}}{\text{cm}^3\cdot\text{K}^2}$	0.198	0.169	0.146	0.157	0.165	0.220
$\Delta(0)$, meV	6.8	7.1	5.9	3.7	4.6	5.0
$\frac{2\Delta(0)}{k_B T_C}$	3.72	3.69	3.64	3.60	3.61	3.65 1
$H_C(0)$, T	0.5	0.5	0.4	0.3	0.3	0.4
Electron transfer, e per H atom	0.625	0.625	0.625	0.667	0.667	0.667

Parameter	La$_3$MgH$_{16}$ 150 GPa	LaMg$_3$H$_{28}$ 200 GPa	LaMg$_3$H$_{28}$ 250 GPa	LaMg$_3$H$_{28}$ 250 GPa
λ	0.76	1.27	1.15	1.09
$\omega_{\log}$, K	1214	1397	1511	1583
ω_2, K	1660	1760	1961	2079
T_C (McM), K	51	134	128	124
T_C (A-D), K	54	149	141	136
T_C (E), K	55	164	157	138
N_f, $\frac{\text{states}}{\text{Ry·Å}^3}$	0.138	0.102	0.116	0.126
γ, $\frac{\text{mJ}}{\text{cm}^3\cdot\text{K}^2}$	0.139	0.133	0.144	0.151
$\frac{\Delta C}{T_C}$, $\frac{\text{mJ}}{\text{cm}^3\cdot\text{K}^2}$	0.243	0.335	0.342	0.332
$\Delta(0)$, meV	8.9	31.3	28.9	24.4
$\frac{2\Delta(0)}{k_B T_C}$	3.75	4.41	4.28	4.11
$H_C(0)$, T	0.7	2.3	2.2	2.0
Electron transfer, e per H atom	0.688	0.321	0.321	0.321

T_C was calculated using McMillan (McM), Allen-Dynes (A-D) formulas, and numerical solution of Eliashberg equations (E) with the Coulomb pseudopotential $\mu^* = 0.1$.
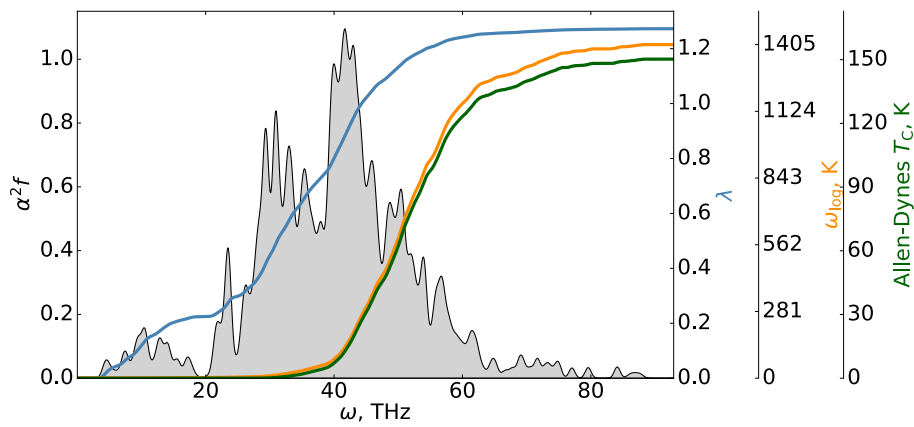
Fig. 4. Eliashberg function, EPC constant λ, logarithmic average frequency $\omega_{\log}$ and critical transition temperature of $LaMg_3H_{28}$ at 200 GPa.

(a) $P2/m$-$LaMgH_8$

(b) $C2/m$-La_2MgH_{12}

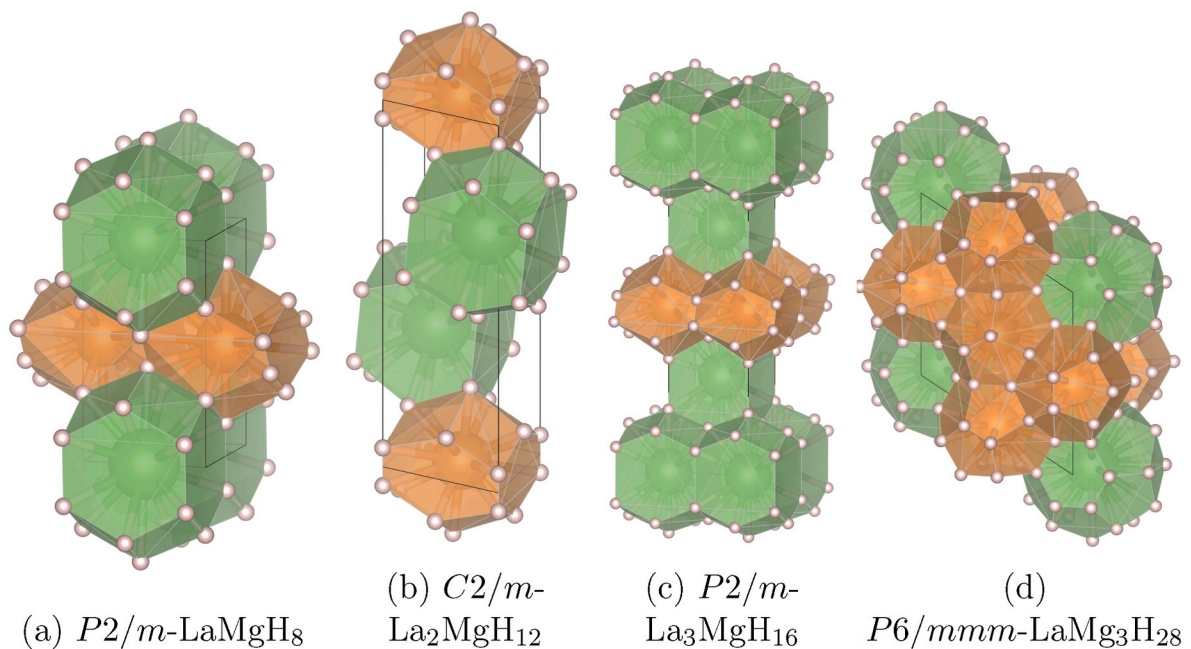(c) $P2/m$-La_3MgH_{16}

(d) $P6/mmm$-$LaMg_3H_{28}$

Fig. 5. Crystal structures of ternary La–Mg–H hydrides.

polyhedra. In addition to such similarity, their EPC constants λ have close values and vary from $\lambda = 0.60$ to $\lambda = 0.77$ (see Table 2). Their T_Cs also have close values: from $T_C = 24$ K to $T_C = 55$ K.

Structure of $LaMg_3H_{28}$ has higher symmetry and higher La and Mg coordination numbers. Superconducting critical temperature of $LaMg_3H_{28}$ is the highest in the whole La–Mg–H system studied and is equal to $T_C = 164$ K at 200 GPa and $T_C = 157$ K at 250 GPa. Its Eliashberg function is presented in Fig. 4.

Superconducting properties of hydrides in the La–Mg–H system can be explained by degree of electron transfer per hydrogen atom. Its values are demonstrated in Tables 1 and 2. If the transfer is low (0–0.13e per H atom), then hydrogen atoms form H–H molecules and one observes molecular hydrides. Indeed, this is what happens in MgH_{26}, MgH_{30}, MgH_{38} and LaH_{23}. They have lower T_C in comparison to other hydrides with higher transfer. If electron transfer is high (≈ 1e per H atom), then hydrogen atoms become hydride ions H$^-$ and one obtains ionic hydrides or subhydrides with no superconductivity, as it is observed in Mg_6H_{11}. It has been shown [45] that high T_C values correspond to intermediate values of electron transfer around 0.33e per H atom. This is confirmed in the La–Mg–H system. $LaMg_3H_{28}$ is the hydride with the highest T_C in the system and it has the transfer of 0.321e per H atom. Other ternary

La–Mg–H hydrides with transfer of ≈ 0.6–0.7e per H atom have significantly lower T_C.

4. Conclusions

We have found several novel lanthanum and magnesium binary hydrides which are thermodynamically stable at 150, 200, 250 and 300 GPa. Novel binary $R\bar{3}m$-LaH_{13} have T_Cs above 100 K. Novel binary $P1$-MgH_{26}, $Fmm2$-MgH_{30} and $P1$-MgH_{38} have T_Cs below 22 K and crystal structures which are very similar to previously reported [17] $R\bar{3}$-MgH_{12} and $P\bar{1}$-MgH_{16}. T_Cs of most ternary La–Mg–H hydrides are below 100 K. However, superconducting critical temperature of $P6/mmm$-$LaMg_3H_{28}$ is 164 K at 200 GPa, which makes this novel ternary hydride a high-temperature superconductor.

We note that predicted ternary hydrides in La–Mg–H system have lower T_C than hydrides in other ternary systems such as $CaYH_{12}$ with theoretically predicted $T_C = 258$ K [51] or $(La,Y)H_{10}$ with experimentally determined $T_C = 253$ K [8]. Nevertheless, the La–Mg–H system has not been previously studied either theoretically or experimentally, while being a combination of promising La–H and Mg–H binary systems. We predict novel stable ternary hydrides in this system and analyze their

superconducting properties. In addition, we confirm that for the ternary La–Mg–H system, a higher T_C corresponds to electron transfer close to 0.33e, as it was previously reported for the binary systems [45].

We also demonstrate that variable-composition searches in pseudo-binary sections play a crucial role in the exploration of complex chemical spaces. Indeed, most of discovered thermodynamically stable ternary hydrides were initially found on pseudobinary convex hulls. This has recently been explored in the COPEX method for compound prediction [52]. Such searches improve ternary diagrams while being less computationally expensive, so we propose them as an important and useful method in any ternary system exploration.

CRediT authorship contribution statement

Grigoriy M. Shutov: Formal analysis, Investigation, Methodology, Validation, Visualization, Writing – original draft, Writing – review & editing. **Dmitrii Semenok:** Conceptualization, Formal analysis, Funding acquisition, Methodology, Project administration, Supervision. **Ivan A. Kruglov:** Conceptualization, Funding acquisition, Project administration, Software, Supervision, Methodology, Resources. **Artem R. Oganov:** Conceptualization, Funding acquisition, Methodology, Project administration, Resources, Software, Supervision.

Declaration of competing interest

The authors declare that they have no known competing financial interests or personal relationships that could have appeared to influence the work reported in this paper.

Data availability

No data was used for the research described in the article.

Acknowledgements

Appendix A. Supplementary data

Supplementary data to this article can be found online at https://doi.org/10.1016/j.mtphys.2023.101300.

References

[1] N. Ashcroft, Metallic hydrogen: a high-temperature superconductor? Phys. Rev. Lett. 21 (1968) 1748–1749, https://doi.org/10.1103/PhysRevLett.21.1748.

[2] A. Drozdov, M. Eremets, I. Troyan, V. Ksenofontov, S. Shylin, Conventional superconductivity at 203 kelvin at high pressures in the sulfur hydride system, Nature 525 (2015) 73–76, https://doi.org/10.1038/nature14964.

[3] A. Drozdov, P. Kong, V. Minkov, S. Besedin, M. Kuzovnikov, S. Mozaffari, L. Balicas, F. Balakirev, D. Graf, V. Prakapenka, E. Greenberg, D. Knyazev, M. Tkacz, M. Eremets, Superconductivity at 250 K in lanthanum hydride under high pressures, Nature 569 (2019) 528–531, https://doi.org/10.1038/s41586-019-1201-8.

[4] M. Somayazulu, M. Ahart, A.K. Mishra, Z.M. Geballe, M. Baldini, Y. Meng, V. V. Struzhkin, R.J. Hemley, Evidence for superconductivity above 260 K in lanthanum superhydride at megabar pressures, Phys. Rev. Lett. 122 (2) (2019): 027001, https://doi.org/10.1103/PhysRevLett.122.027001.

[5] A. Kvashnin, D. Semenok, I. Kruglov, I. Wrona, A. Oganov, High-temperature superconductivity in a Th-H system under pressure conditions, ACS Appl. Mater. Interfaces 10 (2018) 43809–43816, https://doi.org/10.1021/acsami.8b17100.

[6] I. Troyan, D. Semenok, A. Kvashnin, A. Sadakov, O. Sobolevskiy, V. Pudalov, A. Ivanova, V. Prakapenka, E. Greenberg, A. Gavriliuk, I. Lyubutin, V. Struzhkin, A. Bergara, I. Errea, R. Bianco, M. Calandra, F. Mauri, L. Monacelli, R. Akashi,

[7] D. Semenok, I. Kruglov, I. Savkin, A. Kvashnin, A. Oganov, On distribution of superconductivity in metal hydrides, Curr. Opin. Solid State Mater. Sci. 24 (2020): 100808, https://doi.org/10.1016/j.cossms.2020.100808.

[8] D. Semenok, I. Troyan, A. Ivanova, A. Kvashnin, I. Kruglov, M. Hanfland, A. Sadakov, O. Sobolevskiy, K. Pervakov, I. Lyubutin, K. Glazyrin, N. Giordano, D. Karimov, A. Vasiliev, R. Akashi, V. Pudalov, A. Oganov, Superconductivity at 253 K in lanthanum–yttrium ternary hydrides, Mater. Today 48 (2021) 18–28, https://doi.org/10.1016/j.mattod.2021.03.025.

[9] W. Chen, X. Huang, D.V. Semenok, S. Chen, D. Zhou, K. Zhang, A.R. Oganov, T. Cui, Enhancement of superconducting properties in the La–Ce–H system at moderate pressures, Nat. Commun. 14 (1) (2023) 1–8, https://doi.org/10.1038/s41467-023-38254-6.

[10] J. Bi, Y. Nakamoto, P. Zhang, K. Shimizu, B. Zou, H. Liu, M. Zhou, G. Liu, H. Wang, Y. Ma, Giant enhancement of superconducting critical temperature in substitutional alloy (La, Ce) H$_9$, Nat. Commun. 13 (1) (2022) 5952, https://doi.org/10.1038/s41467-022-33743-6.

[11] Y. Song, J. Bi, Y. Nakamoto, K. Shimizu, H. Liu, B. Zou, G. Liu, H. Wang, Y. Ma, Stoichiometric ternary superhydride LaBeH$_8$ as a new template for high-temperature superconductivity at 110 K under 80 GPa, Phys. Rev. Lett. 130 (26) (2023): 266001, https://doi.org/10.1103/PhysRevLett.130.266001.

[12] S. Di Cataldo, C. Heil, W. von der Linden, L. Boeri, LaBH$_8$: towards high-T$_c$ low-pressure superconductivity in ternary superhydrides, Phys. Rev. B 104 (2) (2021) L020511, https://doi.org/10.1103/PhysRevB.104.L020511.

[13] X. Liang, A. Bergara, X. Wei, X. Song, L. Wang, R. Sun, H. Liu, R.J. Hemley, L. Wang, G. Gao, et al., Prediction of high-T$_c$ superconductivity in ternary lanthanum borohydrides, Phys. Rev. 104 (13) (2021) 134501, https://doi.org/10.1103/PhysRevB.104.134501.

[14] I. Kruglov, D. Semenok, H. Song, R. 's, I. Wrona, R. Akashi, M. Davari, D. Duan, T. Cui, A. Kvashnin, A. Oganov, Superconductivity of LaH$_{10}$ and LaH$_{16}$ polyhydrides, Phys. Rev. B 101 (2020): 024508, https://doi.org/10.1103/PhysRevB.101.024508.

[15] D. Laniel, F. Trybel, B. Winkler, F. Knoop, T. Fedotenko, S. Khandarkhaeva, A. Aslandukova, T. Meier, S. Chariton, K. Glazyrin, et al., High-pressure synthesis of seven lanthanum hydrides with a significant variability of hydrogen content, Nat. Commun. 13 (2022) 6987, https://doi.org/10.1038/s41467-022-34755-y.

[16] H. Liu, I. Naumov, R. Hoffmann, N. Ashcroft, R. Hemley, Potential high-T$_c$ superconducting lanthanum and yttrium hydrides at high pressure, Proc. Natl. Acad. Sci. USA 114 (2017) 6990–6995, https://doi.org/10.1073/pnas.1704505114.

[17] D. Lonie, J. Hooper, B. Altintas, E. Zurek, Metallization of magnesium polyhydrides under pressure, Phys. Rev. B Condens. Matter 87 (2013) 1–8, https://doi.org/10.1103/PhysRevB.87.054107.

[18] X. Feng, J. Zhang, G. Gao, H. Liu, H. Wang, Compressed sodalite-like MgH$_6$ as a potential high-temperature superconductor, RSC Adv. 5 (2015) 59292–59296, https://doi.org/10.1039/C5RA11459D.

[19] A. Oganov, C. Glass, Crystal structure prediction using ab initio evolutionary techniques: principles and applications, J. Chem. Phys. 124 (2006).

[20] A. Oganov, A. Lyakhov, M. Valle, How evolutionary crystal structure prediction works-and why, Accounts Chem. Res. 44 (2011) 227–237, https://doi.org/10.1021/ar1001318.

[21] A. Lyakhov, A. Oganov, H. Stokes, Q. Zhu, New developments in evolutionary structure prediction algorithm USPEX, Comput. Phys. Commun. 184 (2013) 1172–1182, https://doi.org/10.1016/j.cpc.2012.12.009.

[22] G. Kresse, J. Furthm'uller, Efficient iterative schemes for ab initio total-energy calculations using a plane-wave basis set, Phys. Rev. B 54 (1996) 11169–11186, https://doi.org/10.1103/PhysRevB.54.11169.

[23] G. Kresse, Ab initio molecular dynamics for liquid metals, J. Non-Cryst. Solids 192–193 (1995) 222–229, https://doi.org/10.1016/0022-3093(95)00355-X.

[24] G. Kresse, J. Hafner, Ab initio molecular-dynamics simulation of the liquid-metal–amorphous-semiconductor transition in germanium, Phys. Rev. B 49 (1994) 14251–14269, https://doi.org/10.1103/PhysRevB.49.14251.

[25] P. Hohenberg, W. Kohn, Inhomogeneous electron gas, Phys. Rev. 136 (1964) B864–B871, https://doi.org/10.1103/PhysRev.136.B864.

[26] W. Kohn, L. Sham, Self-consistent equations including exchange and correlation effects, Phys. Rev. 140 (1965) A1133–A1138, https://doi.org/10.1103/PhysRev.140.A1133.

[27] J. Perdew, K. Burke, M. Ernzerhof, Generalized gradient approximation made simple, Phys. Rev. Lett. 77 (1996) 3865–3868, https://doi.org/10.1103/PhysRevLett.77.3865.

[28] P. Bl'ochl, Projector augmented-wave method, Phys. Rev. B 50 (1994) 17953–17979, https://doi.org/10.1103/PhysRevB.50.17953.

[29] G. Kresse, D. Joubert, From ultrasoft pseudopotentials to the projector augmented-wave method, Phys. Rev. B 59 (1999) 1758–1775, https://doi.org/10.1103/PhysRevB.59.1758.

[30] A. Togo, I. Tanaka, First principles phonon calculations in materials science, Scripta Mater. 108 (2015) 1–5, https://doi.org/10.1016/j.scriptamat.2015.07.021.

[31] A. Ganose, A. Jackson, D. Scanlon, Sumo: command-line tools for plotting and analysis of periodic ab initio calculations, J. Open Source Softw. 3 (2018) 717, https://doi.org/10.21105/joss.00717.

[32] Y. Hinuma, G. Pizzi, Y. Kumagai, F. Oba, I. Tanaka, Band structure diagram paths based on crystallography, Comput. Mater. Sci. 128 (2017) 140–184, https://doi.org/10.1016/j.commatsci.2016.10.015.

[33] P. Giannozzi, S. Baroni, N. Bonini, M. Calandra, R. Car, C. Cavazzoni, D. Ceresoli, G. Chiarotti, M. Cococcioni, I. Dabo, A. Corso, S. Gironcoli, S. Fabris, G. Fratesi,

R. Gebauer, U. Gerstmann, C. Gougoussis, A. Kokalj, M. Lazzeri, L. Martin-Samos, N. Marzari, F. Mauri, R. Mazzarello, S. Paolini, A. Pasquarello, L. Paulatto, C. Sbraccia, S. Scandolo, G. Sclauzero, A. Seitsonen, A. Smogunov, P. Umari, R. Wentzcovitch, Quantum espresso: a modular and open-source software project for quantum simulations of materials, J. Phys. Condens. Matter 21 (2009): 395502, https://doi.org/10.1088/0953-8984/21/39/395502.

[34] S. Baroni, S. Gironcoli, A. Dal, P. Giannozzi, Phonons and related crystal properties from density-functional perturbation theory, Rev. Mod. Phys. 73 (2001) 515–562, https://doi.org/10.1103/RevModPhys.73.515.

[35] J. Perdew, A. Zunger, Self-interaction correction to density-functional approximations for many-electron systems, Phys. Rev. B 23 (1981) 5048–5079, https://doi.org/10.1103/PhysRevB.23.5048.

[36] C. Hartwigsen, S. Goedecker, J. Hutter, Relativistic separable dual-space Gaussian pseudopotentials from H to Rn, Phys. Rev. B 58 (1998) 3641–3662, https://doi.org/10.1103/PhysRevB.58.3641.

[37] P. Allen, R. Dynes, Transition temperature of d-f-band superconductors, Phys. Rev. B 8 (1973) 1079–1087, https://doi.org/10.1103/PhysRevB.8.1079.

[38] G. Eliashberg, Interactions between electrons and lattice vibrations in a normal metal, J. Exp. Theor. Phys. 34 (1960) 996–1001.

[39] P. Allen, R. Dynes, Transition temperature of strong-coupled superconductors reanalyzed, Phys. Rev. B 12 (1975) 905–922, https://doi.org/10.1103/PhysRevB.12.905.

[40] GitGreg228, A2f. URL https://github.com/GitGreg228/a2f.

[41] J. Carbotte, Properties of boson-exchange superconductors, Rev. Mod. Phys. 62 (1990) 1027–1157, https://doi.org/10.1103/RevModPhys.62.1027.

[42] V. Minkov, S. Bud'ko, F. Balakirev, V. Prakapenka, S. Chariton, R. Husband, H. Liermann, M. Eremets, Magnetic field screening in hydrogen-rich high-temperature superconductors, Nat. Commun. 13 (2022) 3194, https://doi.org/10.1038/s41467-022-30782-x.

[43] M. Kuzovnikov, V(p) Equations of State of Novel Lanthanum and Yttrium Superhydrides, ELBRUS, 2021.

[44] K. Momma, F. Izumi, Vesta 3 for three-dimensional visualization of crystal, volumetric and morphology data, J. Appl. Crystallogr. 44 (2011) 1272–1276, https://doi.org/10.1107/S0021889811038970.

[45] F. Peng, Y. Sun, C. Pickard, R. Needs, Q. Wu, Y. Ma, Hydrogen clathrate structures in rare earth hydrides at high pressures: possible route to room-temperature superconductivity, Phys. Rev. Lett. 119 (2017): 107001, https://doi.org/10.1103/PhysRevLett.119.107001.

[46] P. Loubeyre, F. Occelli, P. Dumas, Synchrotron infrared spectroscopic evidence of the probable transition to metal hydrogen, Nature 577 (7792) (2020) 631–635, https://doi.org/10.1038/s41586-019-1927-3.

[47] W. Chen, D. Semenok, A. Kvashnin, X. Huang, I. Kruglov, M. Galasso, H. Song, D. Duan, A. Goncharov, V. Prakapenka, et al., Synthesis of molecular metallic barium superhydride: pseudocubic BaH_{12}, Nat. Commun. 12 (2021) 273, https://doi.org/10.1038/s41467-020-20103-5.

[48] D. Semenok, W. Chen, X. Huang, D. Zhou, I. Kruglov, A. Mazitov, M. Galasso, C. Tantardini, X. Gonze, A. Kvashnin, et al., Sr-doped superionic hydrogen glass: synthesis and properties of SrH_{22}, Adv. Mater. 34 (2022): 2200924, https://doi.org/10.1002/adma.202200924.

[49] D. Semenok, in: Synthesis, X-Ray Diffraction and Nuclear Magnetic Resonance Studies of Cesium and Rubidium Polyhydrides, 6th International Conferenceon Matter and Radiation at Extremes, Zhuhai, Guangdong, China, 2023.

[50] M. Kuzovnikov, in: Synthesis of Novel Rubidium Superhydrides under High Pressure, the Joint 28th AIRAPT and 60th EHPRG International Conference on High Pressure Science and Technology, 2023. Edinburgh, UK.

[51] X. Liang, A. Bergara, L. Wang, B. Wen, Z. Zhao, X.-F. Zhou, J. He, G. Gao, Y. Tian, Potential high-T_c superconductivity in $CaYH_{12}$ under pressure, Phys. Rev. B 99 (10) (2019): 100505, https://doi.org/10.1103/PhysRevB.99.100505.

[52] X. Liu, H. Niu, A.R. Oganov, COPEX: co-evolutionary crystal structure prediction algorithm for complex systems, npj Comp. Mater. 7 (2021) 199, https://doi.org/10.1038/s41524-021-00668-5.